Repair of bone defects using a new biomimetic construction fabricated by adipose-derived stem cells, collagen I, and porous beta-tricalcium phosphate scaffolds

Pei Yang[1], Xin Huang[2], Chunsheng Wang[1], Xiaoqian Dang[1] and Kunzheng Wang[1]

[1]Department of Orthopaedics, the Second Affiliated Hospital of Xi'an Jiaotong University Health Science Center, Xi'an, Shaanxi 710004, China; [2]Department of Cardiology, the First Affiliated Hospital of Xi'an Jiaotong University Health Science Center, Xi'an, Shaanxi 710061, China

Corresponding author: Kunzheng Wang. Email: kunzhengwang@126.com

Abstract

Adipose derived stem cells (ASCs) with multilineage differentiation capacities have been demonstrated as an alternative cell candidate for *in vitro* and *in vivo* bone regeneration. This suggests that they may be a potential candidate to repair the bone defects. We attempted to demonstrate the use of new biomimetic constructions of undifferentiated rabbit adipose-derived stem cells (rASCs) with fully interconnected porous beta-tricalcium phosphate (β-TCP) scaffolds encapsulated by collagen I hydrogel in the regeneration of a critical-sized defect of rabbit radii. Critical-sized defects in the left radii of rabbits were prepared and inserted with rASCs/collagen I/β-TCP scaffold composites or collagen I/β-TCP scaffold composites. The results were evaluated by histology, radiographs, micro-CT, Emission Computed Tomography (ECT), fluorochrome labeling, western blot, and mechanical testing at 4, 8, and 12 weeks postsurgery. Twelve weeks after implantation, the defects were almost completely repaired as confirmed by the presence of the cortical bone and medullary cavity, which was evaluated through radiologic, histologic, and biomechanical examination. Biodegradation of the biomaterials may be attributed to extracellular liquid dissolution together with cell-mediated phagocytosis. Our study shows that a greater number of rASCs in the porous β-TCP scaffold encapsulated by collagen I gel enhanced osteogenesis in critical-sized defects. We hope to garner new insight into the engineering of rASCs-based bone tissue for clinical application.

Keywords: Stem cells-adipose, scaffolds, tissue engineering, bone graft

***Experimental Biology and Medicine* 2013; 238: 1331–1343. DOI: 10.1177/1535370213505827**

Introduction

Although bone has the capacity for regenerative growth and remodeling, these processes are often impaired in clinical situations in which loss of bone is caused by disease, trauma, or tumor resection. More than 800,000 patients receive bone grafts operations annually around the world.[1] The current standard of bone defect repair techniques is allograft, autograft, or artificial bone grafting.[2–6] Allogenic bone grafting technique is widely used in orthopedic and maxillofacial surgery although some disadvantages such as delayed union or non-union, transmitted diseases, and microdamage accumulation are presented.[5,7,8] Though autologous bone grafting technique is viewed as the 'gold standard' for its therapeutic safety and efficacy, many complications such as wound problem, vessel injuries, and bleeding require a secondary surgical operation.[9–11]

This leads us to the development of a scaffold that would provide a suitable environment for tissue development without detrimental effects on surrounding tissues. The ideal scaffold would be facilitated to the attachment of seeded cells to favor growth and subsequent differentiation and revascularization. Furthermore, the scaffold should be osteoconductive, inductive, and osteointegrate with the host bone; have the potential to biodegrade while being gradually replaced by the new bone; be adaptable to an irregularly shaped defect and support mechanical loading; and be storable and able to be sterilized without loss of properties.[1,12–14]

Biomaterials like beta-tricalcium phosphate (β-TCP) have been shown to be an effective composition material candidate for three-dimensional scaffolds, due to its favorable biocompatibility and chemical composition, osteoconductivity, and bioresorbability.[15,16] A porous macro- and microstructure β-TCP scaffold with smooth macropore walls and a smooth implant surface has been in development due to these desirable properties.[15,17,18]

Bone-marrow derived mesenchymal stem cells (BMSCs) have also been exhibited as a potential novel method for cell-based bone tissue engineering; furthermore, adipose-derived stem cells (ASCs) demonstrate similar multilineage differentiation potencies.[19,20] The use of ASCs rather than BMSCs may be advantageous in that greater cell numbers can be harvested from the patient with less pain. As well, both *in vitro* and *in vivo* experiment, ASCs have also been shown to produce osteoid.[21,22]

In this study, we engineered a novel biomimetic bone tissue construct with MSCs isolated from rabbit adipose-derived stem cells (rASCs), using collagen I hydrogel to encapsulate the β-TCP scaffolds designed to enlarge the cells adhesion. The application of this construct to accelerate bone healing was also evaluated with an *in vivo* rabbit model of critical-sized defects.

Materials and methods

In vitro experiment

rASCs isolation and flow cytometry. An aseptic cut of rabbit adipose tissue was performed, and ASCs were extracted in accordance with the conventional method.[23] The third passage of rASCs (P3 rASCs) was obtained for evaluating the osteogenic differentiation capacity using flow cytometry. Briefly, P3 rASCs were trypsinized and incubated with fluorescein-conjugated antibody against CD29, CD34, CD44, and CD45 (Santa Cruz, CA, USA) at 4°C in 0.5% Bovine serum albumin (BSA) and 2 mM Ethylenediaminetetraacetic acid (EDTA) in Phosphate buffered saline (PBS) for 30 min. Subsequently, the labeled cells were run on a BD FACSCanto II flow cytometer (BD, CA, USA) to confirm the phenotypes.

Osteogenic differentiation. Osteogenic induction experiments were conducted using previous methods with minor modifications.[24] At week 2 of culture, alkaline phosphatase (ALP) calcium cobalt staining was conducted, and at week 4 of culture, alizarin red staining was conducted.

Scaffold construction and characterization. The porous β-TCP scaffolds (Cuboid shape: [4 mm × 4 mm × 15 mm]; sterilized by γ radiation) were the products of Shanghai Bio-lu Biomaterials Co., Ltd (Shanghai, China). The basic physical and chemical characterizations of the scaffold are given in Table 1. Four β-TCP scaffold ultrastructures were examined using scanning electron microscopy (SEM) and an additional four scaffolds were decalcified and prepared into 25-mm-thick sections to examine the two-dimensional structure inside the scaffold.

Construction of rASCs/collagen I/β-TCP scaffold composites and collagen I/β-TCP scaffold composites. Ninety-six β-TCP scaffolds were separately placed into an individual well of 12-well plates with 3 mL Dulbecco's Modified Eagle Medium (DMEM) containing 4 mg/mL Collagen I (BD, MA, USA) and incubated for 2 h at 37°C to facilitate hydrogel formation to construct the collagen I/β-TCP scaffold composites. Four collagen I/β-TCP scaffold composites were examined by SEM and 40 were stored at −20°C until use.

The remaining 52 collagen I/β-TCP scaffold composites were removed to new 12-well plates in separate wells. The density of the P3 rASCs was adjusted to be 2×10^4/mL and the cells were seeded into the collagen I/β-TCP scaffold composites with 0.5 mL in each. After 7 days co-culture in 5% CO_2 and 37°C, the rASCs/collagen I/β-TCP scaffold composites were ready for use. Specially, four rASCs/collagen I/β-TCP scaffold composites were removed, respectively, at 3 days and 7 days during co-culturing, and after conventional treatment, SEM was adopted to evaluate the composites structure of cells and scaffolds.

In vivo experiment

Rabbit radial segmental bone defects and study groups. This study was approved under the guidelines of the Institutional Animal Review Committee of Xi'an Jiaotong University. Eighty-eight Japanese White Rabbits (male, age: 6 months; weight: 3.0–3.5 kg) were utilized in this study, and a 15-mm osteoperiosteal defect was generated in the left radius as described previously[2] (Figure 1(a)).

Group A ($n = 44$): The defects were inserted with rASCs/collagen I/β-TCP scaffold composites (Figure 1(b)); group B ($n = 40$), the defects were inserted with collagen I/β-TCP scaffold composites. Group C ($n = 4$) was used as a blank control with no implantation. Internal and external fixations of the operative limbs were unnecessary due to the fibro-osseous union of ulna and radius of rabbit and it will stabilize the implants.

Incisions were then closed with a 1-0 fiber thread suture line in a routine fashion. The animals were monitored postoperatively; enrofloxacin (50 mg/kg) was given for prophylaxis for infection for 5 days. At the respective time point, the rabbits were sacrificed and the left radius–ulnar complexes were obtained.

Radiographic imaging evaluation. At 4, 8, and 12 weeks postsurgery ($n = 4$ for each group), the bone defect healing was assessed based on the scoring system[25] (Table 2) under the standard anteroposterior position X-ray image (Kodak, NY, USA). Bone repair and callus growth status were also evaluated from the gross samples.

Table 1 Physical and chemical properties of the porous β-TCP scaffold

Porosity (%)	Macropore diameter (μm)	Interconnection diameter (μm)	Interconnected pore (%)	Mechanical strength (MPa)	Heavy metal content (ppm)			
					Sn	Ge	Hg	Pb
75.35 ± 6.63	460.90 ± 78.75	157.66 ± 37.94	>99	2.34 ± 0.21	≤3	≤5	≤5	≤30

Micro-CT evaluation. For group A and B, four left radius–ulnar complexes were obtained at 12 weeks postsurgery, fixed in 10% neutral buffered formalin (NBF), and scanned using the micro-CT (GE healthcare, NJ, USA). Thirty-two slices for each millimeter (15 μm with 15 μm gap) were obtained. The bone mineral density (g/cm^2) of the defect region was analyzed by the instrument-provided software based on the different Computed tomography (CT) values of the scaffold and bone.

Fluorochrome labeling. To prepare for fluorescence analysis, the animals were injected with tetracycline (30 mg/kg) at 2 weeks and 3 days prior to their respective sacrifice time point ($n = 4$ in group A and B). After the animals were sacrificed, the samples were obtained for fluorescence analysis.

ECT analysis. The ECT examination was carried out at each time point postsurgery ($n = 4$ in group A and B). Briefly, ^{99m}Tc MDP (18.5 MBq/kg) was injected 4 h prior to the static images were obtained (scanning parameter: 1 frame/5 min, 256×256 matrix). Rectangular regions of interests (ROIs) (1.5×1.5 cm) were drawn in the bone defect areas. The uptake ratio of ^{99m}Tc-MDP (T/NT) of the ROIs was calculated to evaluate the metabolic activity and vascularization of the implants.

Histological evaluation. At each time point postsurgery ($n = 4$ in group A and B), the implants and some surrounding tissues were obtained. After conventional processing, five sequential 8 μm sections per implant were obtained and stained for morphometric analysis under a light microscope (Leica Microsystems, Inc., Germany). The instrument-provided software was used to analyze all slides. Five parameters that included total defect area, new bone area (NBA), new bone volume fraction (NBVF), residual β-TCP area (RTA), and residual β-TCP volume fraction (RTVF) were identified by two independent observers as described previously.[26]

SEM observation of the degeneration of the scaffolds. Four implants of group A at 8 weeks postsurgery were examined by SEM to observe the manner of degeneration of the scaffolds in the ultrastructure.

Western blot analysis of in vivo bone morphogenetic protein 2 (BMP-2) and osteoprotegerin (OPG) protein expression. After retrieval from the rabbits, the composites ($n = 4$ for group A and B at each time point) were used for western blot analysis as described previously[27] for detection of BMP-2 and OPG expression (antirabbit BMP-2 and OPG polyclonal antibody [Beijing Zhongshan, Beijing, China]); the β-actin (Sigma, MO, USA) was selected as internal control.

Biomechanical evaluation. Twelve weeks postoperatively, mechanical evaluation was measured by a three-point bending test as previously reported[1] (methods see supplement document).

Results

In vitro experiments

Isolation, osteogenic differentiation of rASCs. Flow cytometry demonstrated that the cultured P3 rASCs were expressed for CD 29 and CD 44, while not for CD 34 and CD 45 (Figure S1). These phenotypes are similar to those previously reported.[28] rASCs held the morphology of fibroblastoid mononuclear cells (Figure 2(a)). After osteogenic induction, ALP activity and mineralized matrix deposition were confirmed by ALP staining (Figure 2(b)) and alizarin red staining (Figure 2(c)).

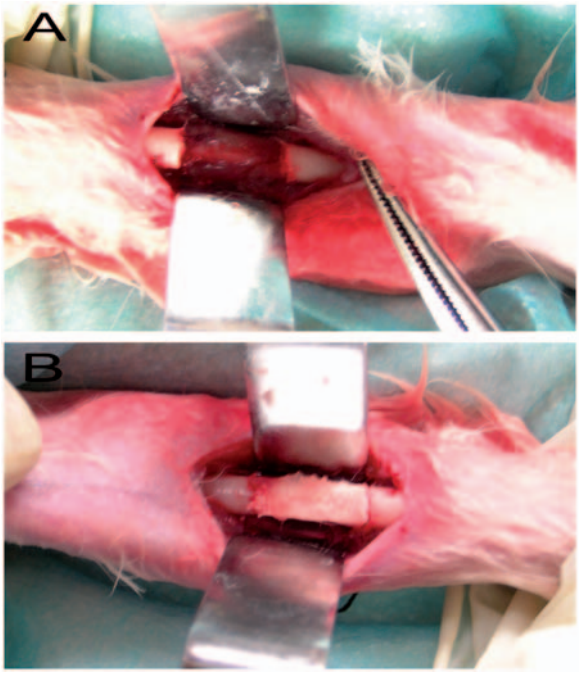

Figure 1 A critical sized (15 mm) segmental defect was created on the left radius of each rabbit (a) and the composites were implanted (b). (A color version of this figure is available in the online journal)

Table 2 Lane–Sandhu radiographic scoring system

	Classification	Score
Bone formation	None	0
	25% of defect	1
	50% of defect	2
	75% of defect	3
	Full	4
Fracture line	Full fracture line	0
	Partial fracture line	2
	Absent fracture line	4
Bone remodeling	None	0
	Intramedullary canal	2
	Full cortex	4

The scoring system included an evaluation of bone formation (5 levels), persistence of the fracture line (3 levels), and bone remodeling (3 levels).

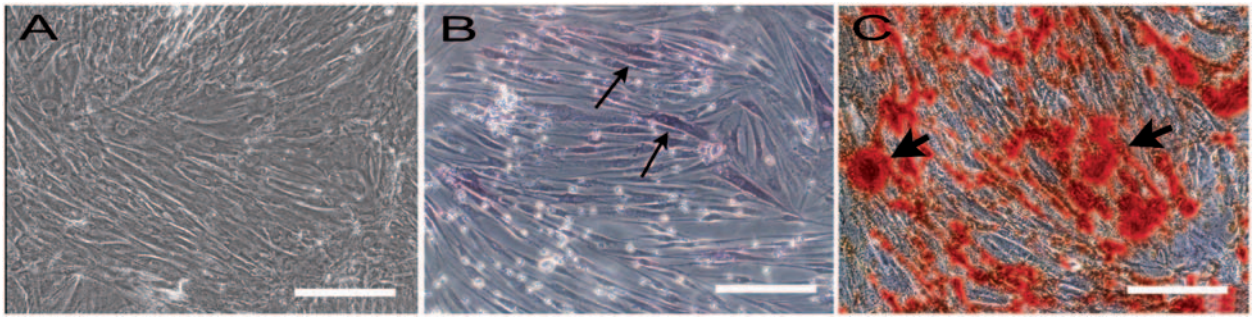

Figure 2 Results of rASC induced to differentiate towards the osteogenic and adipogenic lineages. Morphological observation of rASCs (a). ALP calcium cobalt staining in positive (b) and alizarin red staining in positive (c) after osteogenic induction; Oil Red O staining in positive after adipogenic induction (d). Bars indicate 100 μm. (A color version of this figure is available in the online journal)

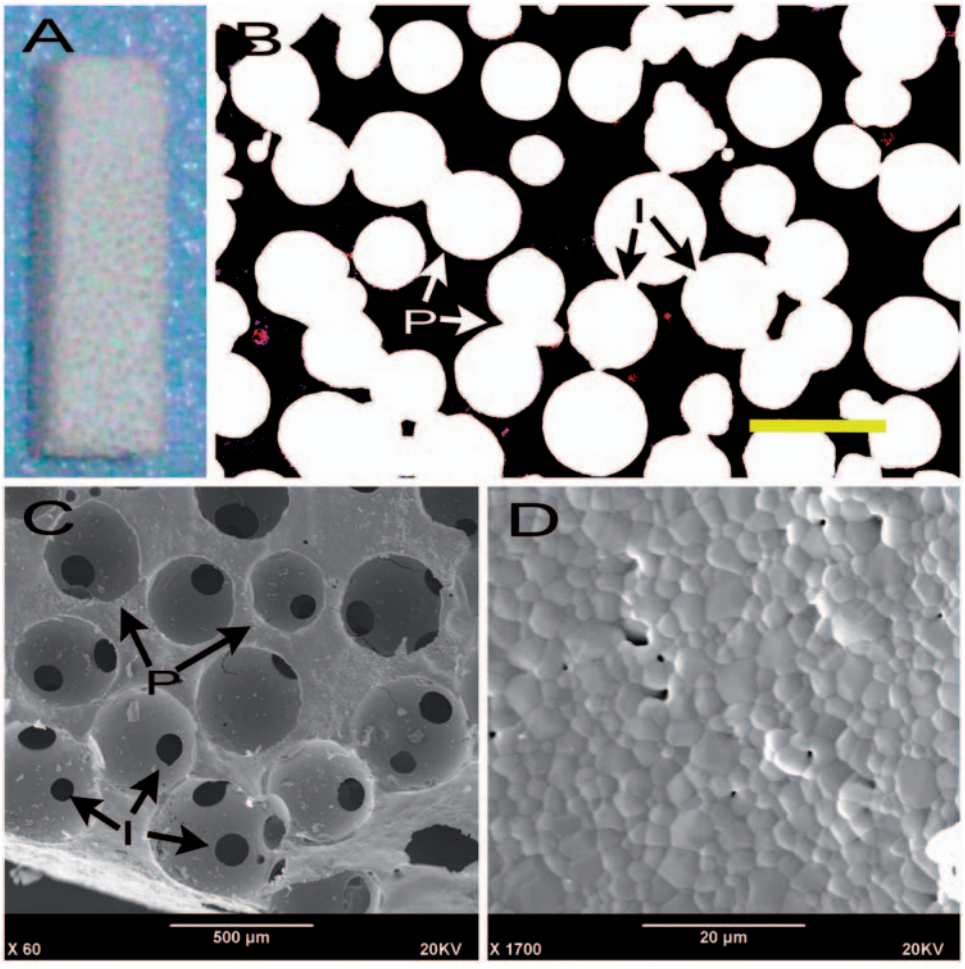

Figure 3 Gross view of β-TCP scaffolds (a). Two-dimensional structure inside the scaffold (b). SEM view of the macrostructure of the porous β-TCP scaffold. Lower magnification of the surface of the scaffold (c). Higher magnification shows the smooth wall of the macropore (d). Bars indicate 500 μm. P, macropore; I, interconnection; S, scaffold. (A color version of this figure is available in the online journal)

Gross view and SEM observation of the β-TCP scaffold. A gross view of the scaffold is shown in Figure 3(a). The two-dimensional structure is depicted in Figure 3(b). Figure 3(c) and (d) is the representative of SEM views of the porous scaffold ultrastructure. The interconnected ratio among the macropores was more than 99% and the wall of scaffold surface and the macropores was smooth as compared to Ca–P cement.

Observation of rASCs/collagen I/β-TCP scaffold composites and collagen I/β-TCP scaffold composites. Figure 4(a) and (b) shows the SEM view of the collagen

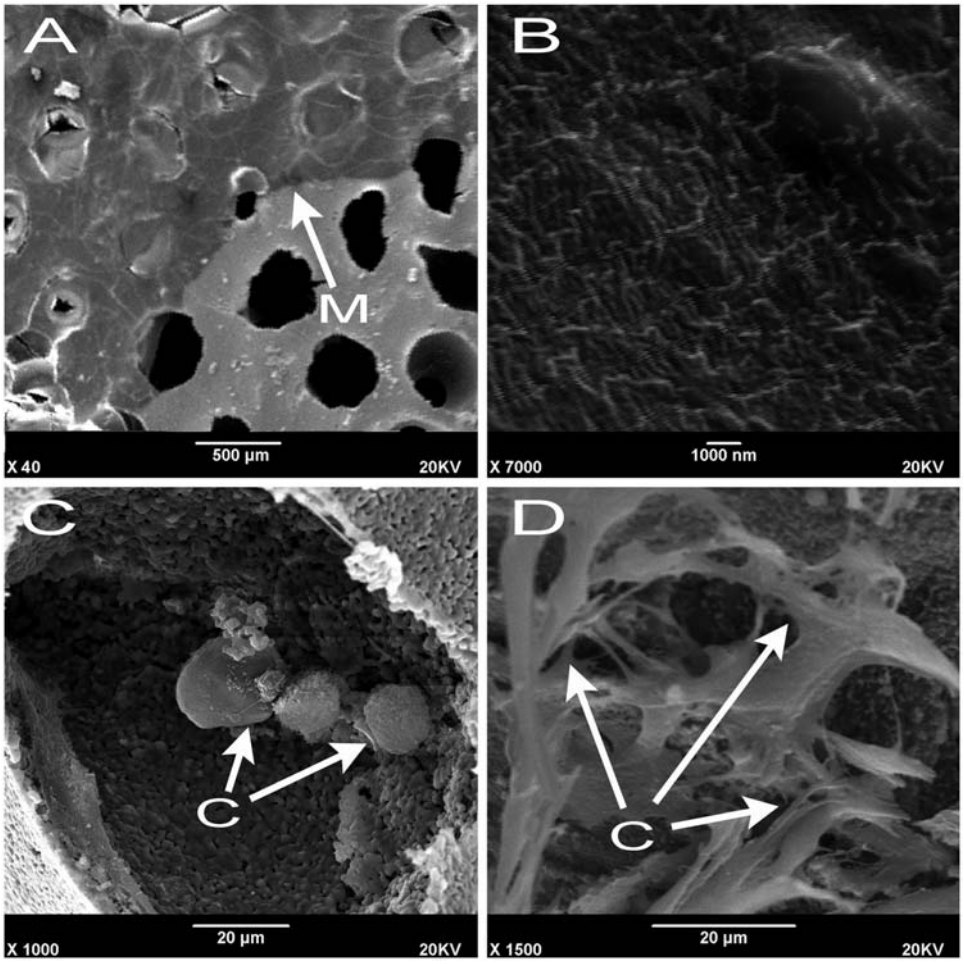

Figure 4 SEM observation of collagen I/β-TCP scaffold composite. Lower magnification (a) and higher magnification (b) of the collagen I hydrogel membrane in the surface of the scaffold. (c) and (d) demonstrated the SEM observation of rASCs/collagen I/β-TCP scaffold composite at 3 days after seeding and 7 days after cell seeding, respectively. M, collagen I hydrogel membrane; C, cell

I/β-TCP scaffold composites. The collagen I hydrogel membrane was observed at the surface of the scaffold. These composites were termed as collagen I/β-TCP scaffold.

At 3 days after the collagen I/β-TCP scaffolds were co-cultured with rASCs, the number of cells with the scaffolds reduced, and cell morphology was not fully extended with a small amount of matrix secretion (Figure 4(c)). At 7 days, the number of composite cells significantly increased, and the morphology was elongated fusiform and fully extended (Figure 4(d)); the cell adhesion to scaffold structure was enhanced.

In vivo experiments

Clinical and physical examinations. Of the 88 rabbits, 85 survived throughout the experiment. Two rabbits in group A and one rabbit in group C died during surgery. The complications such as wound infection and dislocation of the implants were not observed during the whole experiment.

X-ray examinations. At 4 weeks, abundant bone callus was observed around the scaffolds in group A, while group B showed less formation. Furthermore, the boundary of the scaffolds in group B remained clearer than that of group A, demonstrated that the degeneration of scaffolds in group A was faster than group B at the same time point. At 8 weeks postsurgery, new bone extended from both ends of the defects, and only residual β-TCP particles can be observed in the central part of the defect regions. Interestingly, partially radioulnar synostosis was observed due to the bone remodeling. In group B, greater residual β-TCP particles were found that indicated poor osteointegration. At 12 weeks, minimal β-TCP particles were observed throughout the defect regions, and the medullary cavity together with the dorsal cortex of the radii was almost completely reconstructed in group A. While new bone was observed across the defect regions in group B at the same time point, residual β-TCP particles were also present. Group C at each time point postsurgery resulted in non-union, confirming that the defect which we created was of critical size (Figure 5). Significant differences in the radiological scores at each time point postsurgery were observed in all groups. Bone formation was best in group A followed by group B, and lastly group C (Table 3). Gross observation was in accordance with X-ray examinations. (Results see supplement document and Figure S2.)

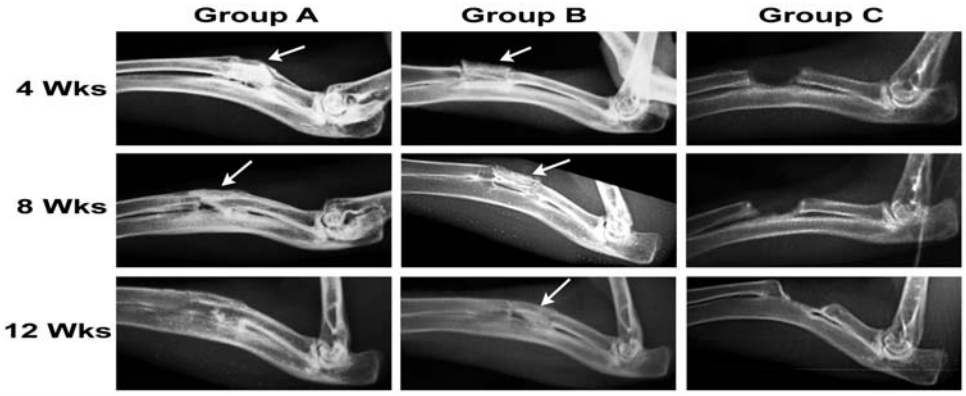

Figure 5 Typical radiographic appearance of defective bridging in rabbit radii of group A, B, and C at each time point

Table 3 The results of Lane–Sandhu radiographic score

	Radiographic score		
Group	**4 weeks**	**8 weeks**	**12 weeks**
Group A	$3.50 \pm 0.50^{*}$	$7.50 \pm 0.50^{*}$	$11.50 \pm 0.50^{*}$†
Group B	1.50 ± 0.50	2.75 ± 0.82	5.50 ± 1.11†
Group C	0.25 ± 0.39†	0.75 ± 0.43	1.25 ± 0.43

*indicate $P < 0.001$ for the rank order of the comparison between groups at 4, 8, and 12 weeks. †indicates a significant difference was found among 4, 8, and 12 scores within the same group (both $P < 0.01$).

Micro-CT evaluation. At 12 weeks postsurgery, based on sagittal and transverse images of the defects and different CT values for bone and the scaffold: in group A, few β-TCP particles were present in the defect regions, and it was notable that the marrow cavity together with the cortical bone of radius were also regenerated (Figure 6(a)); in group B, abundant β-TCP particles were still observed especially in the central part of the defect regions and tight bone connections were not formed (Figure 6(b)). Compared with group B ($0.276 \pm 0.133\ g/cm^2$), the bone mineral density (BMD) in group A ($0.725 \pm 0.181\ g/cm^2$) was significantly higher ($P < 0.01$).

Fluorochrome labeling evaluation. Tetracycline fluorescent labeling was evaluated in groups A and B. Representative fluorescence images of the defect sites and the statistic graph are shown in Figure 7. While both group A and B exhibited increased calcification deposition throughout the study, group B had a significantly lower calcification deposition rate than that of group A at the respective time point ($P < 0.05$). For group A, the difference between 8 weeks and 12 weeks was not significant ($P > 0.05$).

ECT examination. The ECT examination was conducted at each time point postsurgery to assess the metabolic activity and vascularization of the defect region. Static images together with statistic graph were shown in Figure 8. The Target/Non-Target (T/NT) value in the ROIs increased

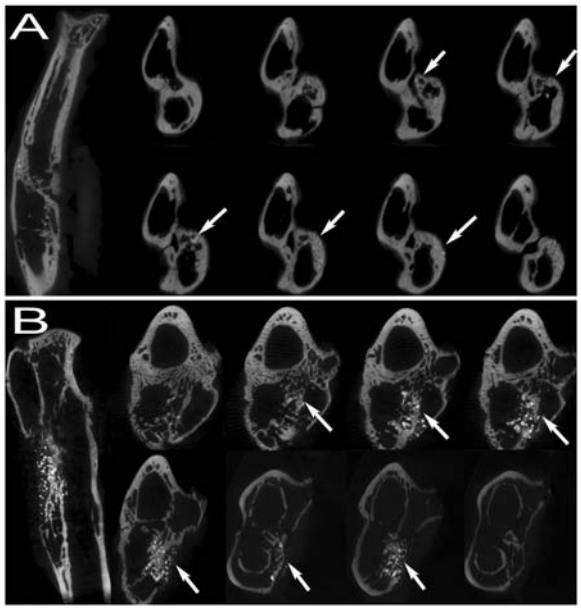

Figure 6 Sagittal and transverse images of the defects by micro-CT of group A (a) and group B (b) at 12 weeks. The white arrow indicates residual β-TCP granules

over the time course of the study postsurgery in both group A and B, while group B had a significantly lower T/NT value than that of group A at the same time point ($P < 0.05$).

Histological examination and quantitative histological analysis. We performed histological analysis to test the osteointegrated efficiency of the host bone tissue and the scaffold together with healing progress of the bone defect. We put emphasis on the histological alterations of the host tissue/implants interface regions and the central part of the implants (Figure 9).

At 4 weeks in group A, the new bone and neocartilage were present not only in the macropores of the host tissue/implants interface regions but also in the macropores of central part of the implants. Fibrous tissues and immature capillaries that are filled with red blood cells were present, which infiltrated between macropores through the

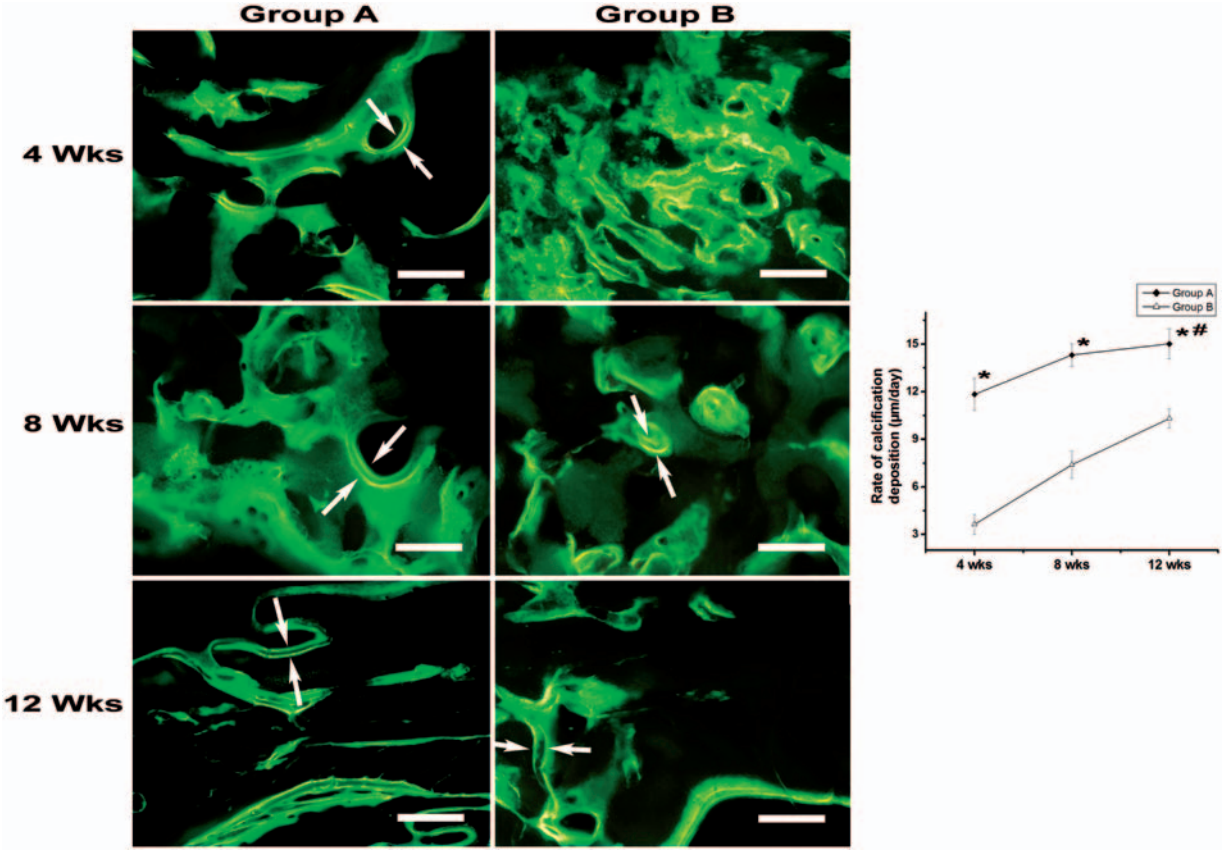

Figure 7 Fluorochrome labeling of bone regeneration of group A and B at 4, 8, and 12 weeks postsurgery. Quantitative analysis of the rate of calcification deposition is also shown. *indicates significant differences between groups at 4, 8, and 12 weeks ($P < 0.05$). #indicates significant difference was not found between 8 weeks and 12 weeks in group A ($P > 0.05$). Bars indicate 300 μm. (A color version of this figure is available in the online journal)

interconnections. Furthermore, negligible degeneration of the scaffolds was observed indicated by the regular blank areas and smooth margins of the macropores. In contrast to group B, very limited new bone was present at the interface regions, and the macropores at the central part of the scaffolds were filled with dense fibroconnective tissues.

At 8 weeks in group A, the margins of the host tissue/implants remained obscure. Abundant mature lamellar bone together with bone marrow components was observed in the macropores and run through the macropores via interconnections across the whole scaffolds. Osteoclasts were also observed, which were responsible for the resorption of the scaffolds and the lamellar bone. Compared to the 4 week time point, the irregular blank areas were present, denoting degeneration of the scaffolds. In group B, the histological appearances were similar to that of group A at 4 weeks. Very limited mature lamellar bone and bone marrow components were observed in the whole scaffolds.

At 12 weeks in group A, compact cortical bones in the dorsal part of the radii together with the regular medullary cavity were almost entirely reconstructed and the scaffolds had almost completely degenerated. In group B, the mature bone and limited bone marrow components were present at the interface regions, while immature bone and fibroconnective tissues were still observed in the central part of the scaffolds. Degeneration of the biomaterials was also observed at this time point; however, the medullary cavity was not yet formed. In group C, as previously mentioned, the defects remained unhealed and sclerosis was also developed.[26]

Statistically, at 4 and 8 weeks, in group A, the NBA and NBVF were greater than that of group B ($P < 0.05$ and $P < 0.01$, respectively). While at 12 weeks, in group A, the NBA and NBVF decreased due to the significant degeneration of the scaffolds and restoration of the marrow cavity ($P < 0.01$, compared with group B) (Figure 10(a) and (b)).

The RTA and RTVF tended to decrease with time postsurgery over the course of the study in both group A and B, while group A had a significantly lower RTA and RTVF than that of group B at 8 and 12 weeks ($P < 0.01$ for each). No statistical difference between group A and B was observed at 4 weeks ($P > 0.05$) (Figure 10(c) and (d)).

SEM observation of the degeneration of the scaffolds. Based on SEM observation, the scaffolds disintegrated into particles that were not more than 5 μm in diameter in group A at 8 weeks, and cell-mediated phagocytosis was observed, which attributed to the biodegradation of the biomaterials (Figure 11).

BMP-2 and OPG protein expression analysis. The expression pattern of BMP-2 and OPG *in vivo* was evaluated by western blot in group A and B at each time point

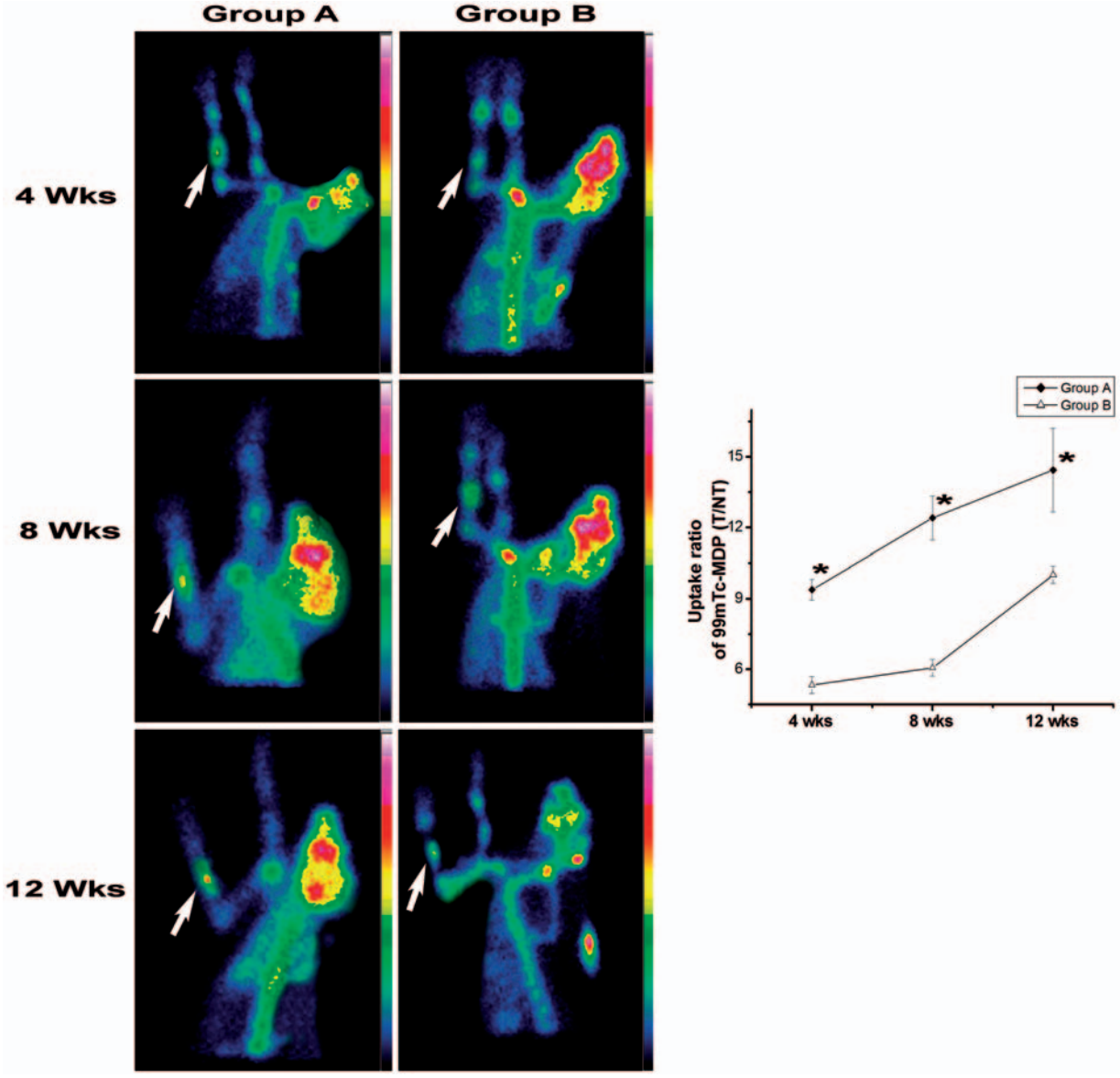

Figure 8 Typical ECT images of group A and B at 4, 8, and 12 weeks postsurgery. Quantitative analysis of the uptake ratio of ^{99m}Tc-MDP (T/NT) is also shown. The white arrow indicates the ROIs. *indicates significant differences between groups at 4, 8, and 12 weeks (both $P < 0.05$). (A color version of this figure is available in the online journal)

postsurgery. As shown in Figure 12, there was increased expression of BMP-2 and OPG in group A than that of group B at each time point (both $P < 0.05$).

Biomechanical evaluation. We carried out three-point bending tests on the radii in group A and B together with the control group (normal radii) 12 weeks postsurgery to assess the mechanical properties of the repaired bone. Group A showed dramatically higher compression strength than group B ([91.21 ± 8.43 N], [39.23 ± 4.58 N] for group A and B, respectively, $P < 0.001$). The control group (102.49 ± 10.22 N) had greater compression strength than group A ($P > 0.05$), and significance was observed between group B and control group ($P < 0.001$).

Discussion

In the study, we engineered a novel biomimetic bone construct by applying collagen I hydrogel and porous β-TCP scaffolds together with rASCs, which were implanted into critical-sized bone defects in the midshaft of rabbit radii. The defects were successfully repaired as exhibited by the presence of medullary cavity and cortical bone by 12 weeks. Biomechanical examination demonstrated the mechanical property of the repaired bone had almost recovered to normal function. Furthermore, cell-mediated phagocytosis was also observed by SEM examination, which is responsible for the biodegradation of the biomaterials.

The study of cell–scaffold or growth factor–scaffold composites *in vitro* and induced tissue and organ regeneration

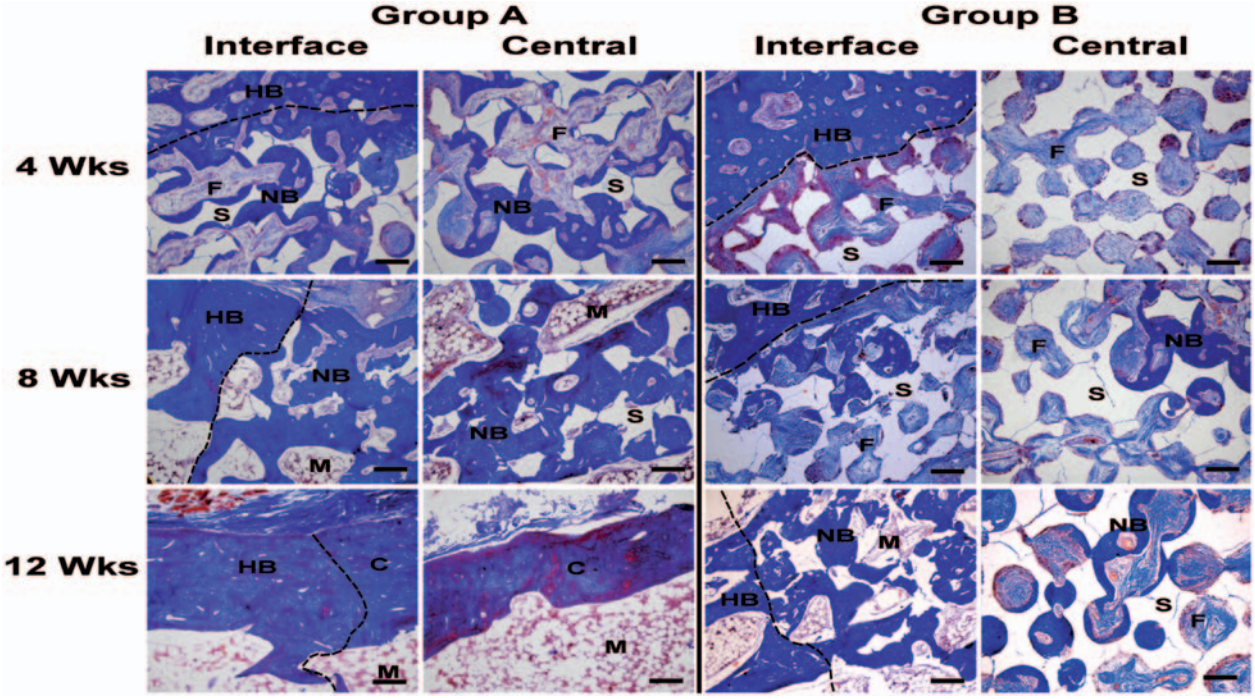

Figure 9 Typical histological appearance of defect bridging in rabbit radii of group A and B at 4, 8, and 12 weeks by Masson-trichrome staining. The broken line shows the interface between host tissues and the implant. The spherical structure shows the macropores of the scaffold. HB, host bone; NB, new bone; C, cortex F, fibrous tissues; M, medullary tissues; S, the shadow of β-TCP produced by decalcification. Bars indicate 300 μm. (A color version of this figure is available in the online journal)

in vivo have been advanced by the development and extensive use of three-dimensional porous biomaterials. Microarchitectures such as porosity, macropore shape, macropore size, and interconnections were critical characteristics to improve the efficiency of the scaffolds.[29,30] Macropores and interconnections between nearby macropores act as two constitutive components of scaffolds, which strongly influence cell migration and tissue penetration.[29–31] Generally, a pore size of less than 150 μm can support the in growth of connective tissue, but is not favorable for osteocytic in growth.[1] Kuboki *et al.* has reported that macropore size between 300 and 900 μm supports the progression of osteogenesis and it can be used in bone tissue engineering fields.[32] It has also been reported that interconnections of at least 150 μm facilitate mineralized bone tissue in growth, whereas osteoid tissue is favored at less than 100 μm, and fibrous tissue at 5–15 μm.[33] Furthermore, studies show new tissue can develop from the surface of a porous material into the inner section if the porosity is greater than 50% and the pores are interconnected.[1,29,30,33] For the β-TCP scaffold we used in the present study, pore size (460.90 ± 78.75 μm) and interconnection pore size (157.66 ± 37.94 μm) were found to be well biocompatible, osteoconductive, and biodegradable, which facilitate vascularization and rapid bone growth progression.[17,32]

Up to date, stem cell-based tissue engineering is focused on bone marrow-derived stromal cells (BMSCs).[1,21,25,34] Despite the controversies, some scholars have described that there are no differences on multilineage differentiation capacities between BMSCs and ASCs.[20,21,35] The ASCs could present the osteogenic potential when co-cultured with β-TCP scaffolds in osteogenic media as confirmed by the detection of the osteocalcin.[36] Other reports have suggested that the biochemical composition of the scaffold may contribute to greater functionality of the engineered tissue construct by influencing ASC differentiation. Compared to a PLA scaffold alone, ASCs-seeded PLA/β-TCP scaffolds have been shown to increase cell-mediated mineralization and ALP activity in the osteogenic media.[37] ASCs are an advantageous cell source over BMSCs for bone tissue engineering in many aspects in that the use of autologous ASCs for minimizing immunological rejection, and greater cell numbers can be harvested from the patient with less pain.[23,24,34]

In this study, collagen I hydrogel was selected to encapsulate the β-TCP scaffolds to facilitate the adhesion of undifferentiated rASCs. Hydrogels such as collagen I are semisolid hydrophilic polymer networks. Collagen I is able to enhance the efficiency of cell adhesion and drug delivery by serving as a biomaterials scaffold to encapsulate large numbers of cells. As well, the permeability of the material allows the transfer of nutrients and oxygen in and metabolities out facilitated by water retention.[38] The enhanced efficiency of cell adhesion was observed based on our SEM results *in vitro*. Some scholars reported that osteogenic predifferentiated ASCs *in vitro* could maintain the phenotype *in vivo* and hold the potential of regenerative properties at a bone defect site, whereas scaffolds seeded with undifferentiated ASCs fail to repair bone defects.[34,39,40]

Based on our radiographic and histological results, abundant new bone together with the osteoblasts was observed throughout the scaffolds at 4 and 8 weeks

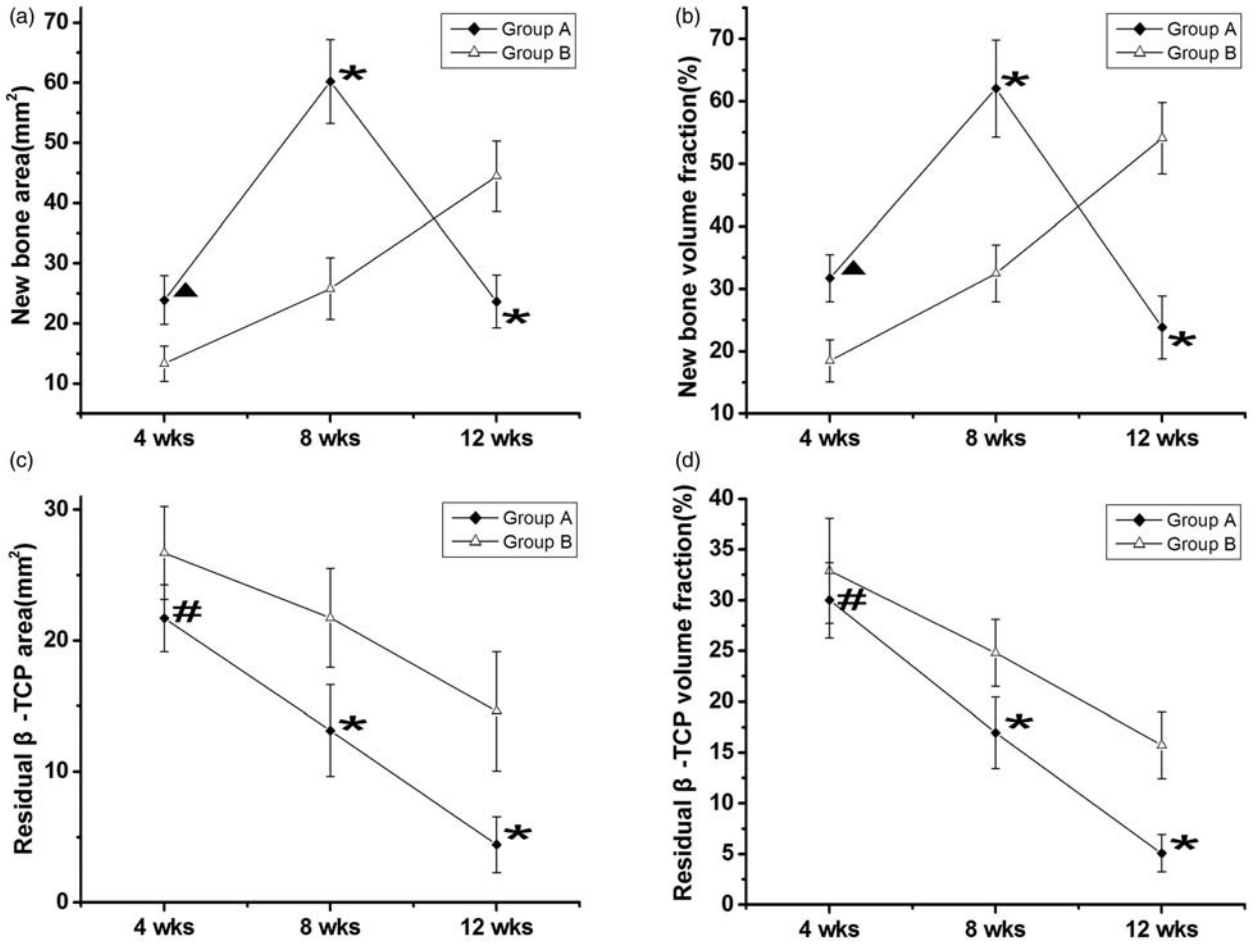

Figure 10 The quantitative histological analysis of new bone area (a), new bone volume fraction (b), residual β-TCP area (c), and residual β-TCP volume fraction (d). * indicates $P < 0.01$ vs. group B at the same time point, indicates $P < 0.05$ vs. group B at the same time point, # indicates $P > 0.05$ vs. group B at the same time point

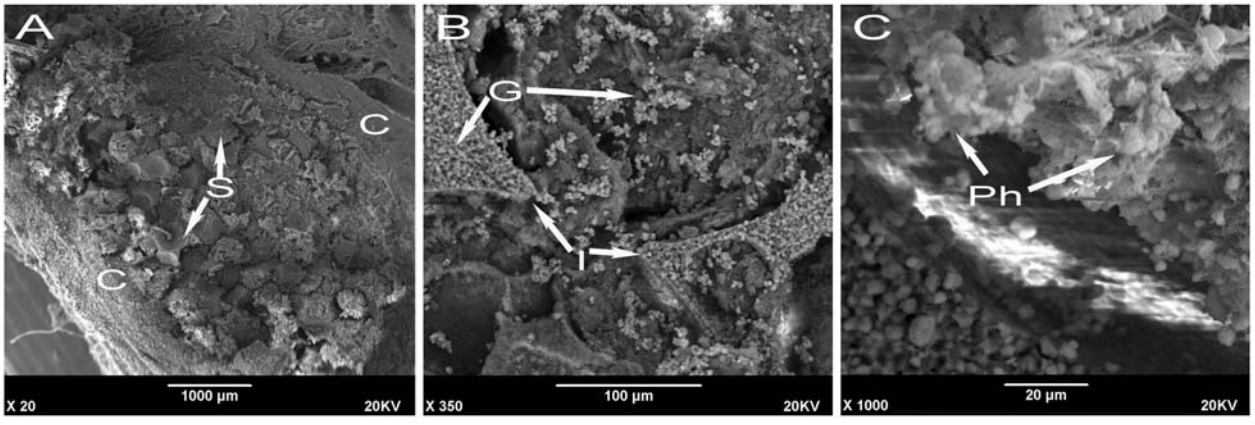

Figure 11 SEM observation of the scaffold in group A at 8 weeks. Lower magnification of the defect area (a). Higher magnification shows the disintegration of the scaffold and phagocytosis phenomenon (b, c). G: β-TCP granules; I, interconnection; S, scaffold; C. cortex; Ph, phagocytosis

postsurgery, as well as considerable mature lamellar bone following treatment with rASCs/collagen I/scaffold constructs. The driving mechanisms that contributed to our results were that: (1) the biochemical composition of the scaffolds aid in the functionality of the construct by directing rASCs differentiation;[36,37] (2) the osteogenic differentiation was enhanced by extrinsic physical stimuli (mechanical or electrical) *in vivo*;[41–43] (3) collagen I could promote adhesion and osteogenic differentiation of BMSCs or ASCs *in vitro* based on its primary organic

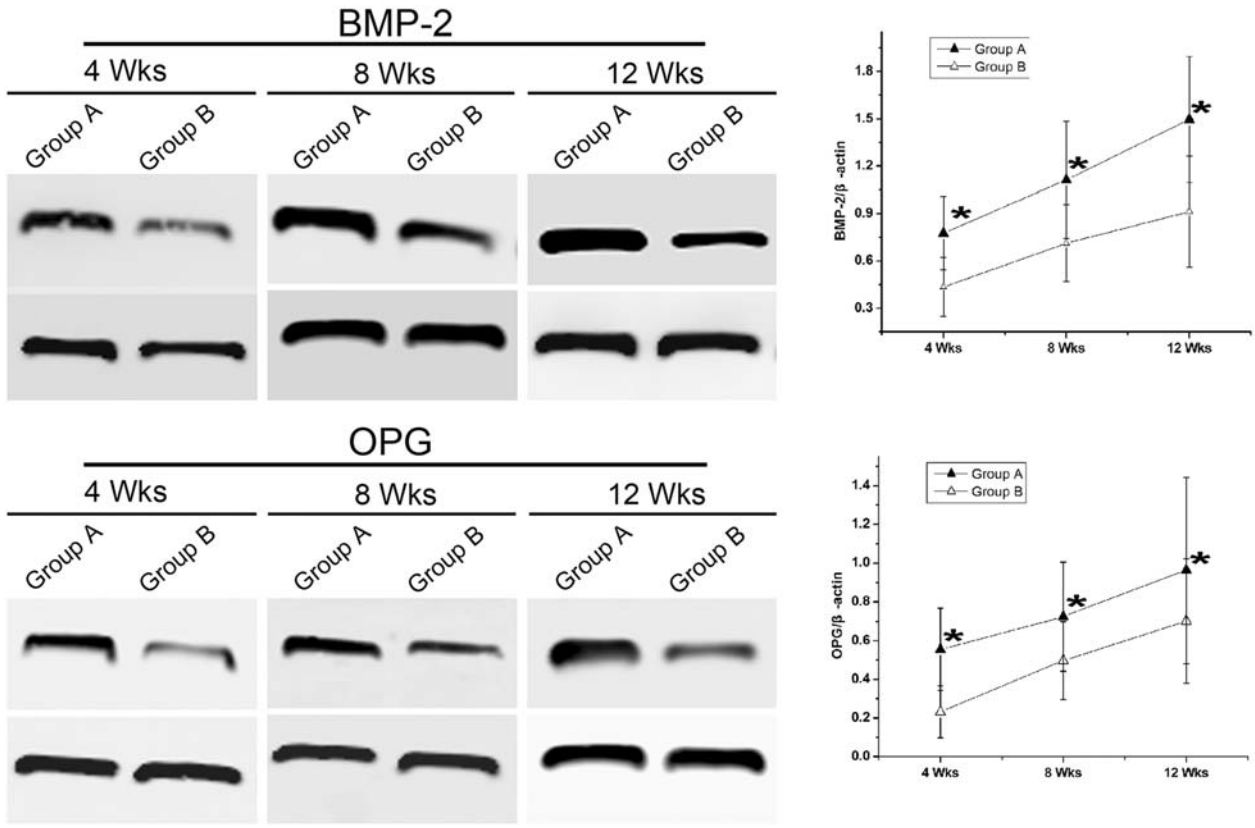

Figure 12 Western blot results of BMP-2 and OPG of each group at 4, 8, and 12 weeks showing increased protein expression in Group A. * indicates $P < 0.05$ vs. group B at the same time point.
BMP-2: morphogenetic protein 2; OPG: osteoprotegerin

component of bone matrices;[44,45] (4) the increased number of recruited host cells enhanced bone tissue formation. Our western blot results demonstrated the increased protein expression of BMP-2 and OPG, which demonstrated the successful *in vivo* osteogenic differentiation of rASCs.

An ideal engineered bone tissue scaffolds should be replaced completely by new bone citing the importance of the balance between the degradation of biomaterial and the formation of bone. If the degeneration rate is too fast, the biomaterial will disintegrate before the new bone formation, which will compromise the repair; however, if the rate is too slow, the formation of new bone, remodeling, and reconstruction will be hindered.[46] In our experiments, the bone defects were almost completely repaired following the implantation with rASCs/collagen I/scaffold constructs, and the scaffolds were also completely degenerated and creeping was substituted by new bone at the proper time based on our X-ray, histology, and micro-CT results. According to our histological and SEM observations, the scaffolds in group A demonstrated ideal degeneration due to the following: (1) differentiation led to rapid angiogenesis and osteogenesis in the scaffolds in group A; (2) the presence of abundant vessels led to the improvement of the extracellular fluid environment (ECT results demonstrated the rapid revascularization process in group A), and extracellular liquid dissolution was the major biodegradation mechanism of the biomaterials we adopted in the present study;[47,48] (3) the scaffolds disintegrated into particles less than 5 μm in diameter, in which cell-mediated phagocytosis was observed to be responsible for the biodegradation of the biomaterials.

Conclusions

The present study shows that enhanced numbers of rASCs in a porous β-TCP scaffold encapsulated in collagen I gel promoted osteogenesis in critical-sized defects. Twelve weeks after implantation, the defects were almost completely repaired by the presence of the cortical bone and medullary cavity. Our results also suggested that the degeneration of the scaffolds may be accelerated by the interaction of rASCs, collagen I, and the biomaterials. We hope to garner new insight into the engineering of rASCs-based bone tissue for clinical application.

Author contributions: PY and KW designed the experiments. PY and CW performed the experiments. XH and XD performed the statistical analysis. PY and KW wrote the manuscript.

ACKNOWLEDGEMENTS

This study was supported by the National Science foundation of China (81000809). We thank Prof. Zongchang He of the

Foreign Language Department Xi'an Jiaotong University for the help in preparing the manuscript.

REFERENCES

1. Wang G, Yang H, Li M, Lu S, Chen X, Cai X. The use of silk fibroin/hydroxyapatite composite co-cultured with rabbit bone-marrow stromal cells in the healing of a segmental bone defect. *J Bone Joint Surg Br* 2010;**92**:320–25
2. Langer R, Vacanti JP. Tissue engineering. *Science* 1993;**260**:920–26
3. Eward WC, Rineer CA, Urbaniak JR, Richard MJ, Ruch DS. The vascularized fibular graft in precollapse osteonecrosis: Is long-term hip preservation possible? *Clin Orthop Relat Res* 2012;**470**:2819–26
4. Gao YS, Ai ZS, Yu XW, Sheng JG, Jin DX, Chen SB, Cheng XG, Zhang CQ. Free vascularised fibular grafting combined with a locking plate for massive bone defects in the lower limbs: A retrospective analysis of fibular hypertrophy in 18 cases. *Injury* 2012;**43**:1090–95
5. Couture J, Cabana F. Irradiated allograft bone in spine surgery: To culture or not? A single center retrospective study. *Spine (Phila Pa 1976)* 2013;**38**:558–63
6. Carter JD, Swearingen AB, Chaput CD, Rahm MD. Clinical and radiographic assessment of transforaminal lumbar interbody fusion using HEALOS collagen-hydroxyapatite sponge with autologous bone marrow aspirate. *Spine J* 2009;**9**:434–38
7. Prolo DJ and Rodrigo JJ. Contemporary bone graft physiology and surgery. *Clin Orthop Relat Res* 1985;**200**:322–42
8. Agholme F, Aspenberg P. Experimental results of combining bisphosphonates with allograft in a rat model. *J Bone Joint Surg Br* 2009;**91**:670–75
9. Damien CJ, Parsons JR. Bone graft and bone graft substitutes: A review of current technology and applications. *J Appl Biomater* 1991;**2**:187–208
10. Bucholz RW. Nonallograft osteoconductive bone graft substitutes. *Clin Orthop Relat Res* 2002;**395**:44–52
11. Van der Stok J, Van Lieshout EM, El-Massoudi Y, Van Kralingen GH, Patka P. Bone substitutes in the Netherlands – a systematic literature review. *Acta Biomater* 2011;**72**:739–50
12. Burg KJ, Porter S, Kellam JF. Biomaterial developments for bone tissue engineering. *Biomaterials* 2000;**21**:2347–59
13. Lin AS, Barrows TH, Cartmell SH, Guldberg RE. Microarchitectural and mechanical characterization of oriented porous polymer scaffolds. *Biomaterials* 2003;**243**:481–89
14. Li S, De Wijn JR, Li J, Layrolle P, De Groot K. Macroporous biphasic calcium phosphate scaffold with high permeability/porosity ratio. *Tissue Eng* 2003;**9**:535–48
15. Kurashina K, Kurita H, Wu Q, Ohtsuka A, Kobayashi H. Ectopic osteogenesis with biphasic ceramics of hydroxyapatite and tricalcium phosphate in rabbits. *Biomaterials* 2002;**232**:407–12
16. Saito M, Shimizu H, Beppu M, Takagi M. The role of beta-tricalcium phosphate in vascularized periosteum. *J Orthop Sci* 2000;**5**:275–82
17. Guo X, Wang C, Duan C, Descamps M, Zhao Q, Dong L, Lü S, Anselme K, Lu J, Song YQ. Repair of osteochondral defects with autologous chondrocytes seeded onto bioceramic scaffold in sheep. *Tissue Eng* 2004;**10**:1830–40
18. Wheeler DL, Chamberland DL, Schmitt JM, Buck DC, Brekke JH, Hollinger JO, Joh SP, Suh KW. Radiomorphometry and biomechanical assessment of recombinant human bone morphogenetic protein 2 and polymer in rabbit radius ostectomy model. *J Biomed Mater Res* 1998;**434**:365–73
19. Haynesworth SE, Goshima J, Goldberg VM, Caplan AI. Characterization of cells with osteogenic potential from human marrow. *Bone* 1992;**13**:81–88
20. De Ugarte DA, Morizono K, Elbarbary A, Alfonso Z, Zuk PA, Zhu M, Dragoo JL, Ashjian P, Thomas B, Benhaim P, Chen I, Fraser J, Hedrick MH. Comparison of multi-lineage cells from human adipose tissue and bone marrow. *Cells Tissues Organs* 2003;**174**:101–9
21. Hattori H, Sato M, Masuoka K, Ishihara M, Kikuchi T, Matsui T, Takase B, Ishizuka T, Kikuchi M, Fujikawa K, Ishihara M. Osteogenic potential of human adipose tissue-derived stromal cells as an alternative stem cell source. *Cells Tissues Organs* 2004;**178**:2–12
22. Hicok KC, Du Laney TV, Zhou YS, Halvorsen YD, Hitt DC, Cooper LF, Gimble JM. Human adipose-derived adult stem cells produce osteoid in vivo. *Tissue Eng* 2004;**10**:371–80
23. Zuk PA, Zhu M, Mizuno H, Huang J, Futrell JW, Katz AJ, Benhaim P, Lorenz HP, Hedrick MH. Multilineage cells from human adipose tissue: implications for cell-based therapies. *Tissue Eng* 2001;**7**:211–18
24. Zuk PA, Zhu M, Ashjian P, De Ugarte DA, Huang JI, Mizuno H, Alfonso ZC, Fraser JK, Benhaim P, Hedrick MH. Human adipose tissue is a source of multipotent stem cells. *Mol Biol Cell* 2002;**13**:4279–95
25. Kern S, Eichler H, Stoeve J, Klüter H, Bieback K. Comparative analysis of mesenchymal stem cells from bone marrow, umbilical cord blood, or adipose tissue. *Stem Cells* 2006;**24**:1294–301
26. Yang P, Wang C, Shi Z, Huang X, Dang X, Li X, Lin SF, Wang K. rhVEGF 165 delivered in a porous beta-tricalcium phosphate scaffold accelerates bridging of critical-sized defects in rabbit radii. *J Biomed Mater Res A* 2010;**92**:626–40
27. Li Z, Liao W, Zhao Q, Liu M, Xia W, Yang Y, Shao N. Angiogenesis and bone regeneration by allogeneic mesenchymal stem cell intravenous transplantation in rabbit model of avascular necrotic femoral head. *J Surg Res* 2013;**183**:193–203
28. Yang Z, Huang CY, Candiotti KA, Zeng X, Yuan T, Li J, Yu H, Abdi S. Sox-9 facilitates differentiation of adipose tissue-derived stem cells into a chondrocyte-like phenotype in vitro. *J Orthop Res* 2011;**29**:1291–97
29. Mastrogiacomo M, Scaglione S, Martinetti R, Dolcini L, Beltrame F, Cancedda R, Quarto R. Role of scaffold internal structure on in vivo bone formation in macroporous calcium phosphate bioceramics. *Biomaterials* 2006;**27**:3230–37
30. De Oliveira JF, De Aguiar PF, Rossi AM, Soares GA. Effect of process parameters on the characteristics of porous calcium phosphate ceramics for bone tissue scaffolds. *Artif Organs* 2003;**27**:406–11
31. Lee M, Wu BM, Dunn JC. Effect of scaffold architecture and pore size on smooth muscle cell growth. *J Biomed Mater Res A* 2008;**87**:1010–16
32. Kuboki Y, Jin Q, Takita H. Geometry of carriers controlling phenotypic expression in BMP-induced osteogenesis and chondrogenesis. *J Bone Joint Surg Am* 2001;**83-A**:S105–15
33. Lu JX, Flautre B, Anselme K, Hardouin P, Gallur A, Descamps M, Thierry B. Role of interconnections in porous bioceramics on bone recolonization in vitro and in vivo. *J Mater Sci Mater Med* 1999;**10**:111–20
34. Bodle JC, Hanson AD, Loboa EG. Adipose-derived stem cells in functional bone tissue engineering: Lessons from bone mechanobiology. *Tissue Eng Part B Rev* 2011;**17**:195–211
35. Tjabringa GS, Vezeridis PS, Zandieh-Doulabi B, Helder MN, Wuisman PI, Klein-Nulend J. Polyamines modulate nitric oxide production and COX-2 gene expression in response to mechanical loading in human adipose tissue-derived mesenchymal stem cells. *Stem Cells* 2006;**24**:2262–69
36. Hattori H, Masuoka K, Sato M, Ishihara M, Asazuma T, Takase B, Kikuchi M, Nemoto K, Ishihara M. Bone formation using human adipose tissue-derived stromal cells and a biodegradable scaffold. *J Biomed Mater Res B Appl Biomater* 2006;**76**:230–39
37. McCullen SD, Zhu Y, Bernacki SH, Narayan RJ, Pourdeyhimi B, Gorga RE, Loboa EG. Electrospun composite poly(L-lactic acid)/tricalcium phosphate scaffolds induce proliferation and osteogenic differentiation of human adipose-derived stem cells. *Biomed Mater* 2009;**4**:035002
38. Lutolf MP, Hubbell JA. Synthetic biomaterials as instructive extracellular microenvironments for morphogenesis in tissue engineering. *Nat Biotechnol* 2005;**23**:47–55
39. Yoon E, Dhar S, Chun DE, Gharibjanian NA, Evans GR. In vivo osteogenic potential of human adipose-derived stem cells/poly lactide-co-glycolic acid constructs for bone regeneration in a rat critical-sized calvarial defect model. *Tissue Eng* 2007;**13**:619–27
40. Jeon O, Rhie JW, Kwon IK, Kim JH, Kim BS, Lee SH. In vivo bone formation following transplantation of human adipose-derived stromal cells that are not differentiated osteogenically. *Tissue Eng Part A* 2008;**14**:1285–94

41. Kearney EM, Farrell E, Prendergast PJ, Campbell VA. Tensile strain as a regulator of mesenchymal stem cell osteogenesis. *Ann Biomed Eng* 2010;**38**:1767–79
42. Sumanasinghe RD, Osborne JA, Loboa EG. Mesenchymal stem cell-seeded collagen matrices for bone repair: Effects of cyclic tensile strain, cell density, and media conditions on matrix contraction *in vitro*. *J Biomed Mater Res A* 2009;**88**:778–86
43. Hanson AD, Marvel SW, Bernacki SH, Banes AJ, van Aalst J, Loboa EG. Osteogenic effects of rest inserted and continuous cyclic tensile strain on hASC lines with disparate osteodifferentiation capabilities. *Ann Biomed Eng* 2009;**37**:955–65
44. Li H, Dai K, Tang T, Zhang X, Yan M, Lou J. Bone regeneration by implantation of adipose-derived stromal cells expressing BMP-2. *Biochem Biophys Res Commun* 2007;**356**:836–82
45. Alonso M, Claros S, Becerra J, Andrades JA. The effect of type I collagen on osteochondrogenic differentiation in adipose-derived stromal cells *in vivo*. *Cytotherapy* 2008;**10**:597–610
46. Zellin G, Gritli-Linde A, Linde A. Healing of mandibular defects with different biodegradable and non-biodegradable membranes: an experimental study in rats. *Biomaterials* 1995;**16**:601–9
47. Kurashina K, Kurita H, Hirano M, Kotani A, Klein CP, de Groot K. In vivo study of calcium phosphate cements: Implantation of an alpha-tricalcium phosphate/dicalcium phosphate dibasic/tetracalcium phosphate monoxide cement paste. *Biomaterials* 1997;**18**:539–43
48. den Hollander W, Patka P, Klein CP, Heidendal GA. Macroporous calcium phosphate ceramics for bone substitution: A tracer study on biodegradation with 45Ca tracer. *Biomaterials* 1991;**12**:569–73

(Received June 6, 2013, Accepted August 5, 2013)